

Supplementary Information for **A Strategy to the Assembly of Functional Small Cations with Layered Double Hydroxides for Luminescence Ultra Thin Films**

Dongpeng Yan,^a Jun Lu,^{a} Li Chen,^a Shengui Qin,^a Jing Ma,^b Min Wei,^{a*} David G. Evans,^a and Xue Duan^a*

^a State Key Laboratory of Chemical Resource Engineering, Beijing University of Chemical Technology, Beijing 100029, P. R. China.

^b School of Chemistry and Chemical Engineering, Key Laboratory of Mesoscopic Chemistry of MOE, Nanjing University, Nanjing 210093, P.R. China.

List of Contents

1. Experimental Details for the (BNMA@PVS/LDH)_n UTFs.

Scheme S1: The assembly process for (BNMA@PVS/LDH)_n UTF.

Table S1: The CIE 1931 color coordinates for the (BNMA@PVS/LDH)_n UTFs.

Figure S1: Absorption and photoluminescence spectrum of BNMA aqueous solution.

2. Structural and morphology characterization of the (BNMA@PVS/LDH)_n UTFs.

Figure S2: XRD patterns for the (BNMA@PVS/LDH)_n UTFs with 8, 16, 24, 32 bilayers.

Figure S3. FT-IR spectra for the cation BNMA and BNMA@PVS/LDH UTF.

Table S2: 2θ degree and d values (\AA) for the (BNMA@PVS/LDH)_n UTFs.

Table S3: Depth and thickness parameters for the UTFs with 8, 16, 24, 32 bilayers.

Figure S4: Side view of SEM image for the BNMA@PVS/LDH UTFs.

3. Fluorescence properties analysis of the (BNMA@PVS/LDH)_n UTFs.

Figure S5: Comparison of fluorescence decay profile for (BNMA@PVS/LDH)₃₂ UTFs and BNMA powder.

Table S4: Fluorescence lifetimes of the (BNMA@PVS/LDH)_n UTFs.

Figure S6: Time decay fluorescence anisotropy for the (BNMA@PVS/LDH)₃₂ UTF.

Table S5: Time-resolved anisotropy parameters for the (BNMA@PVS/LDH)₃₂ UTF

Figure S7: I-V profiles for the BNMA@PVS/LDH UTFs.

4. Calculation details and analysis of the BNMA@PVS/LDH system.

Scheme S2: Structural model of LDH layer, cation (BNMA²⁺) and anion (PVS¹⁰⁻).

Figure S8. MD snapshots of the top view and side view of the BNMA@PVS/LDH system.

Figure S9: The angel distribution of the N–N line of BNMA and end-chain C–C line of PVS respective to the LDH layer.

5. Ordered assembly of the (Rhodamine 6G @PVS/LDH)_n UTFs.

Figure S10: UV-vis absorption and fluorescence spectra of the (Rhodamine 6G@PVS/LDH)_n UTFs.

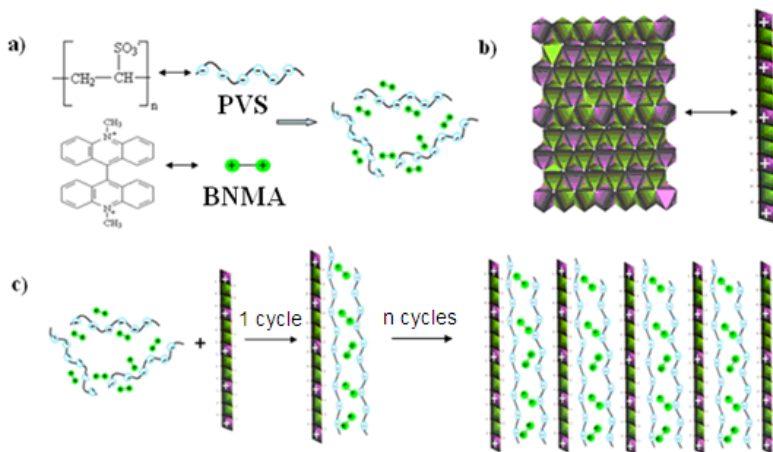
1. Experimental Details for the (BNMA@PVS/LDH)_n UTFs.

Reagents and materials: Analytical pure Mg (NO₃)₂·6H₂O, Al (NO₃)₃·9H₂O and urea were purchased from Beijing Chemical Co. Ltd. and used without further purified. Bis (N-methylacridinium) nitrate (BNMA, M. W. = 353.84), polyvinylsulfonate (PVS, M. W. = 175000), and rhodamine 6G (M. W. = 479.01) were purchased from Sigma Chemical Co. Ltd.

Fabrication of the UTFs: Typically, 0.075 g PVS and 0.0176 g BNMA (*ca.* ten vinylsulfonate units correspond to one BNMA cation) were dissolved in 100 mL of water, named as BNMA@PVS solution. The process of synthesis and exfoliation of Mg-Al-LDH were similar to that described in our previous work.^[1] 0.1 g of Mg-Al-LDH was shaken in 100 cm³ of formamide solution for 24 h to produce a colloidal suspension of exfoliated Mg-Al-LDH nanosheets. The quartz glass substrate was first cleaned in concentrated NH₃/30% H₂O₂ (7:3) and concentrated H₂SO₄ for 30 min each. After such procedure, the quartz substrate was rinsed and washed thoroughly with deionic water. The substrate was then dipped in a colloidal suspension (1 g dm⁻³) of LDH nanosheets for 10 min followed by thoroughly washing, and then the substrate was treated with a 100 mL of BNMA@PVS aqueous solution for 10 min and the washing procedure was the same as that for the LDH nanosheets. Multi-layer films of (BNMA@PVS/LDH)_n were fabricated by depositing alternatively with LDH nanosheets solution and BNMA@PVS solution for *n* cycles. The resulting films were dried under a nitrogen gas flow for 2 min at 25 °C. The nominal composition for the UTFs can be expressed as: Mg₂Al(OH)₆[C₂H₃SO₃)_{0.999}][(C₂₈H₂₂N₂)_{0.001}] (C₂H₃SO₃: one vinylsulfonate units; C₂₈H₂₂N₂: BNMA). The EDX analysis afforded the elemental percentage content of the UTF: Mg: 17.46 %; Al: 10.31 %; C: 18.62 %; S: 10.59 %, from which the observed composition for the UTF can be expressed as: Mg_{1.969}Al_{1.031}(OH)₆[C₂H₃SO₃)_{0.867}][(C₂₈H₂₂N₂)_{0.163}]. To further extend the method above, monovalent cation Rhodamine 6G (R6G) was selected to form R6G@PVS (0.0237g: 0.075g) solution, and then the (R6G@PVS/LDH)_n UTFs were fabricated by the similar assembly process.

Sample characterization: The UV-vis absorption spectra were collected in the range from 190 to 900 nm on a Shimadzu U-3000 spectrophotometer, with the slit width of 1.0 nm. The fluorescence spectra were performed on a RF-5301PC fluorospectrophotometer with the excitation wavelength of 371 nm. The fluorescence emission spectra are in the range from 450 to 630 nm, and both the excitation and emission slit are set to 3.0 nm. The color coordinates

of the fluorescence were determined by PR-650 spectrophotometer. Steady-state polarized photoluminescence measurements of $(\text{BNMA}@\text{PVS}/\text{LDH})_n$ UTFs were recorded with an Edinburgh Instruments' FLS 920 fluorospectrophotometer. The fluorescence decays were measured using LifeSpec-ps spectrometer by 372 nm laser exciting for $(\text{BNMA}@\text{PVS}/\text{LDH})_n$ UTFs, and the lifetimes were calculated with the F900 Edinburgh instruments software. X-ray diffraction patterns (XRD) of the $(\text{BNMA}@\text{PVS}/\text{LDH})_n$ UTFs were recorded using a Rigaku 2500VB2+PC diffractometer under the conditions: 40 kV, 50 mA, Cu K α radiation ($\lambda = 0.154056$ nm) with step-scanned in step of 0.04° (2θ) in the range from 2 to 18° using a count time of 10 s/step. The morphology of UTFs was investigated by using a scanning electron microscope (SEM Hitachi S-3500) equipped with an EDX attachment (EDX Oxford Instrument Isis 300), and the accelerating voltage applied was 20 kV. The surface roughness and thickness data were obtained by using the atomic force microscopy (AFM) software (Digital Instruments, Version 6.12). The I-V profiles for the UTFs were measured by HP4145 semiconductor parameter analyzer.



Scheme S1. a) The chemical formula of Bis (N-methylacridinium) cation (BNMA) and polyvinylsulfonate (PVS), which formed BNMA@PVS pair in solution; b) the representation of one Mg-Al-layered double hydroxide monolayer (Mg-Al-LDH) (dark pink: $\text{Al}(\text{OH})_6$ octahedra; green: $\text{Mg}(\text{OH})_6$ octahedra); and c) the assembly process for $(\text{BNMA}@\text{PVS}/\text{LDH})_n$ UTF.

Table S1: The CIE1931 color coordinates for the $(\text{BNMA}@\text{PVS}/\text{LDH})_n$ UTFs

<i>n</i>	8	16	24	32
CIE 1931	(0.336, 0.445)	(0.335, 0.462)	(0.327, 0.476)	(0.304, 0.534)

CIE 1931 color coordinates for the $(\text{BNMA}@\text{PVS/LDH})_n$ UTFs illustrate that the luminescence of the $(\text{BNMA}@\text{PVS/LDH})_n$ UTFs is populated in the yellow-green region.

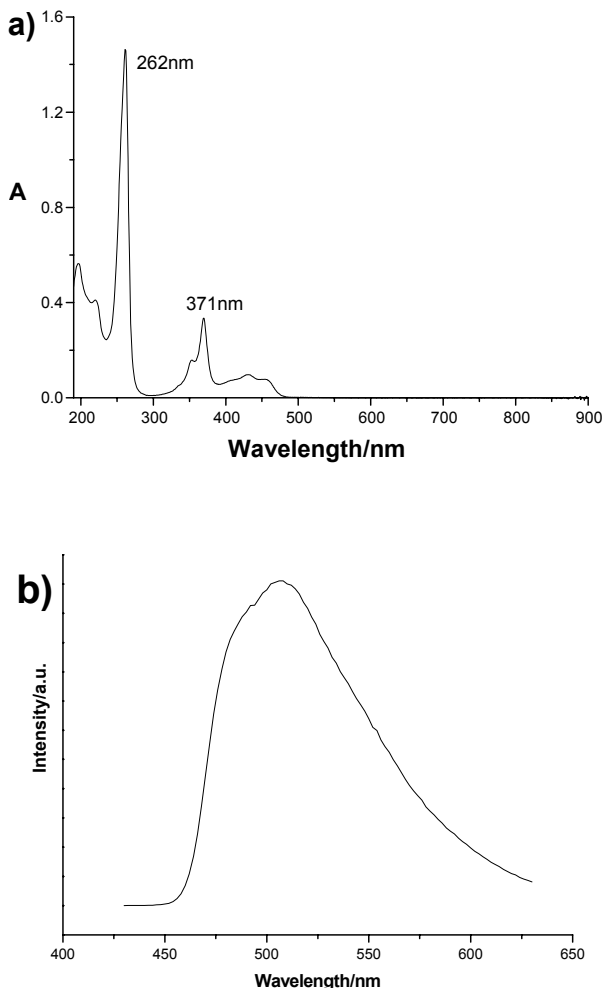


Figure S1. a) absorption and b) fluorescence spectra of the BNMA aqueous solution (10 μM).

The emission peak of the UTFs and solution appear at 510 nm with the full width at half maximum (FWHM) of *ca.* 88 and 84 nm. This may suggest that the environment in the interlayer was similar to that in solution.

2. Structural and morphology characterization of the $(\text{BNMA}@\text{PVS/LDH})_n$ UTFs

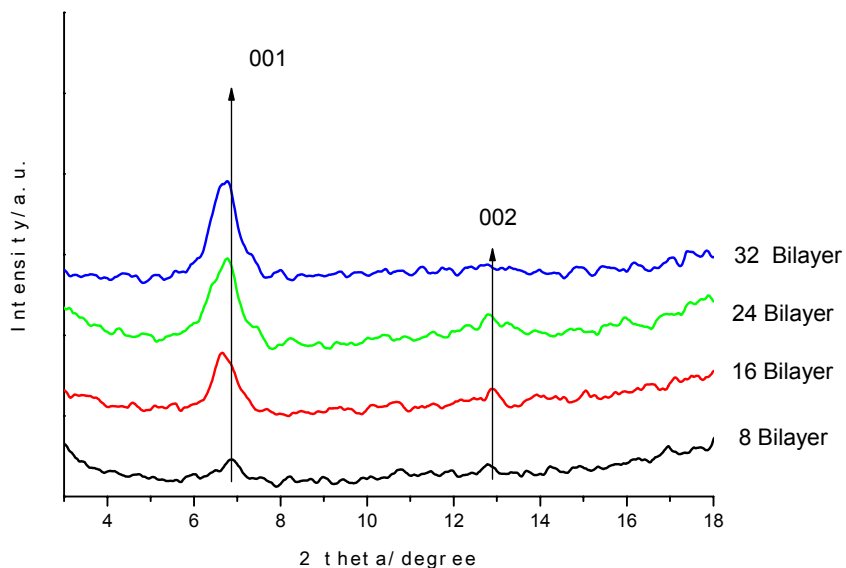


Figure S2. The XRD patterns for the (BNMA@PVS/LDH)_n UTFs with 8, 16, 24, 32 bilayers.

Table S2: Positions of XRD peaks (2θ $^{\circ}$) and d values (\AA) for the (BNMA@PVS/LDH)_n UTFs.

n	8	16	24	32
2θ (degree)	6.91	6.56	6.60	6.77
d (\AA)	12.78	13.46	13.38	13.04

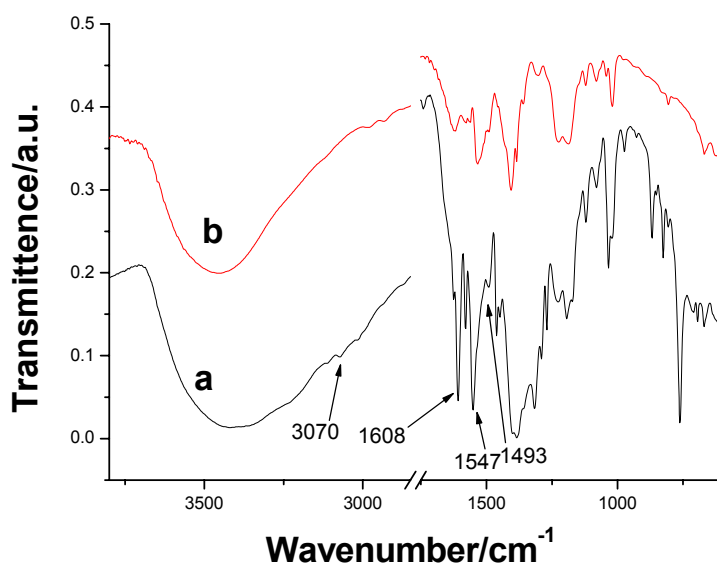


Figure S3. FT-IR spectra for a) the fluorescent cation BNMA; b) BNMA@PVS/LDH UTFs.

The characteristic stretching vibration band of the skeleton vibration of phenyl ring in BNMA appears at 1608, 1547 and 1493 cm⁻¹. The weak band at 3070 cm⁻¹ corresponds to the stretching vibration of C-H in C=C-H. It can be observed that the peak position of the BNMA@PVS/LDH UTF are nearly unchanged compared with that of the pristine fluorescent cation BNMA sample; moreover, the peaks of the film became relative regular respective to the pristine sample, illustrating that the BNMA cation is more structural ordered within the LDH layer.

Table S3: Depth and thickness parameters for the UTFs with 8, 16, 24, 32 bilayers

<i>n</i>	8	16	24	32
rms roughness (nm)^[a]	6.618	8.601	10.488	13.637
SEM thickness (nm)^[b]	ca. 14	ca. 27	ca. 44	ca. 55

^[a]The statistical rms roughness values were obtained by AFM.

^[b]The SEM thickness values were obtained from the side view of (BNMA@PVS/LDH)_{*n*} UTFs, see Figure S3.

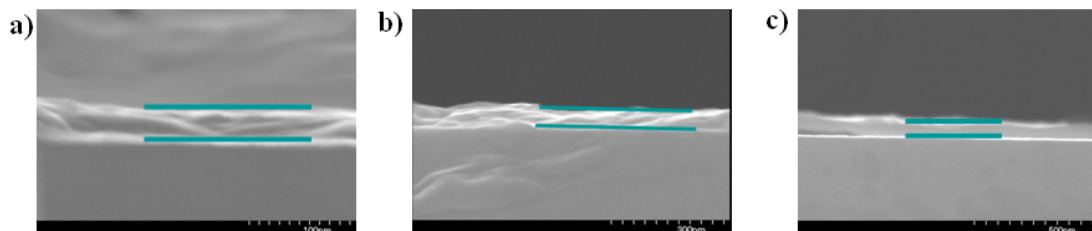


Figure S4. Side view of SEM images for the (BNMA@PVS/LDH)_{*n*} UTFs with a) 16, b) 24, c) 32 bilayers.

3. Fluorescence and electric properties analysis for the (BNMA@PVS/LDH)_{*n*} UTFs.

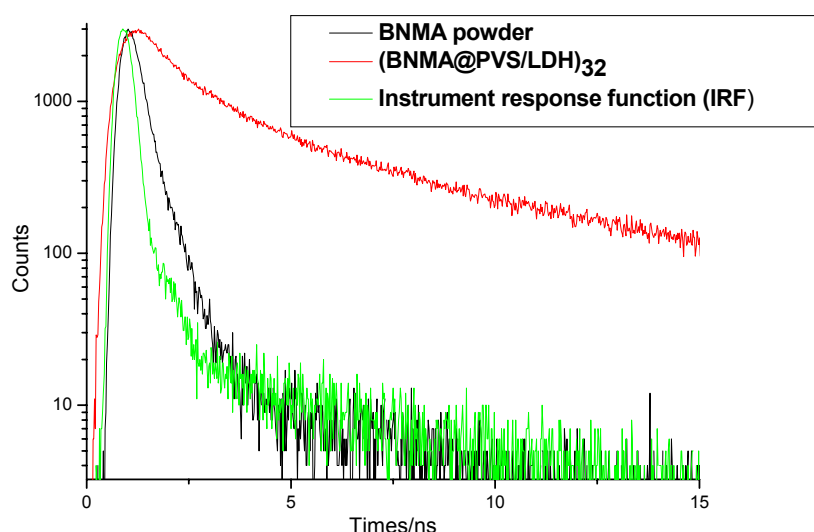


Figure S5. Comparison of fluorescence decay profiles for the $(\text{BNMA}@\text{PVS/LDH})_{32}$ UTF and BNMA powder sample.

Table S4: Fluorescence lifetimes of the $(\text{BNMA}@\text{PVS/LDH})_n$ UTFs

Bilayer number	8	16	24	32
Lifetime τ_I (ns) ^[a]	4.61	4.83	4.88	5.03
χ^2	2.02	3.34	5.62	3.39

^[a] τ_I : the fluorescence lifetime; χ^2 : the fitting goodness.

Time-resolved anisotropy measurement is an important method to investigate the rotation behavior^[2] and energy transfer^[3] of luminous molecules in the time range of their fluorescence lifetime. The fluorescence anisotropy time decay profile for the $(\text{BNMA}@\text{PVS/LDH})_{32}$ UTF is shown in Figure S5. The anisotropy r can be expressed as:^[4]

$$r(t) = \frac{I_{VV}(t) - G(t)I_{VH}(t)}{I_{VV}(t) + 2G(t)I_{VH}(t)}. \quad (1)$$

where I_{VH} stands for the photoluminescence (PL) intensity obtained with vertical excitation polarized and horizontal detection polarization, and I_{VV} , I_{HV} , I_{HH} are defined in a similar way. $G = I_{HV}/I_{HH}$, which was determined from the BNMA aqueous solution.

The rotation behavior can be fitted by the formula as follows:^[4]

$$r(t) = (r_0 - r_\infty)e^{-t/\phi} + r_\infty \quad (2)$$

where r_0 is limiting anisotropy; r_∞ is residual anisotropy and ϕ is orientation correlation time of the BNMA molecule in the gallery of LDH. These values are tabulated in Table S5.

The orientation correlation time (ϕ) is the time that the anisotropy decreases to its $1/e$ of initial value. It can be found that the ϕ of the UTF (1.16 ns) is about 1/4 of the corresponding fluorescence lifetime, suggesting that the flexibility imposed by PVS is favorable for the rotation of the BNMA molecule. The values of limiting anisotropy (r_0) of the UTF are around 0.21, in accordance with the results of steady-state polarization photoemission spectra at this wavelength.

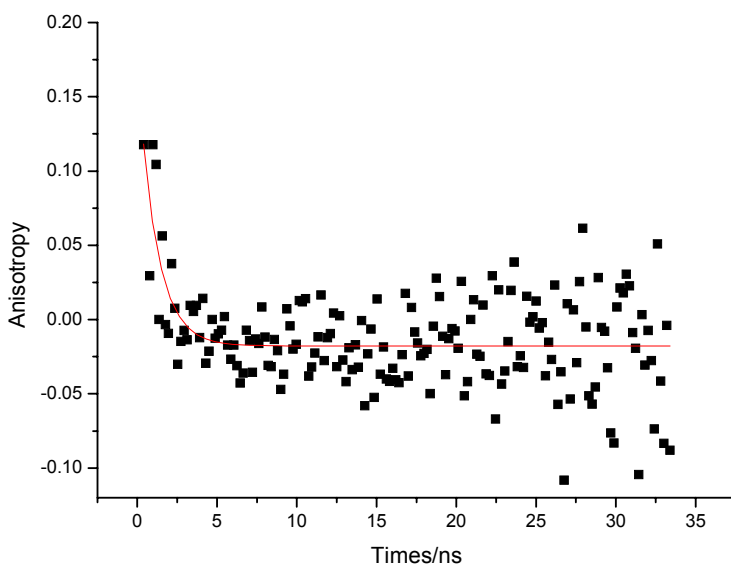


Figure S6. Time decay fluorescence anisotropy for the $(\text{BNMA}@\text{PVS/LDH})_{32}$ UTF.

Table S5: Orientation Correlation Time (φ), Limiting Anisotropy (r_0) and Residual Anisotropy (r_∞) for the $(\text{BNMA}@\text{PVS/LDH})_{32}$ UTF

Orientation correlation time φ (ns)	Limiting anisotropy (r_0)	Residual anisotropy(r_∞)
1.160	0.208	-0.018

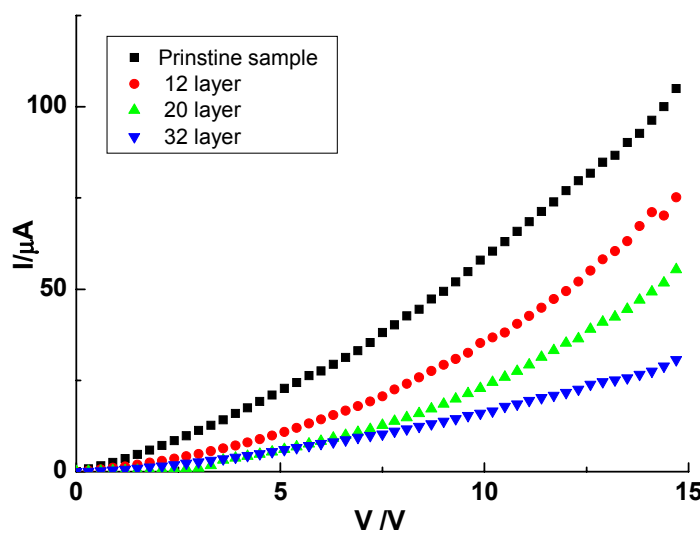
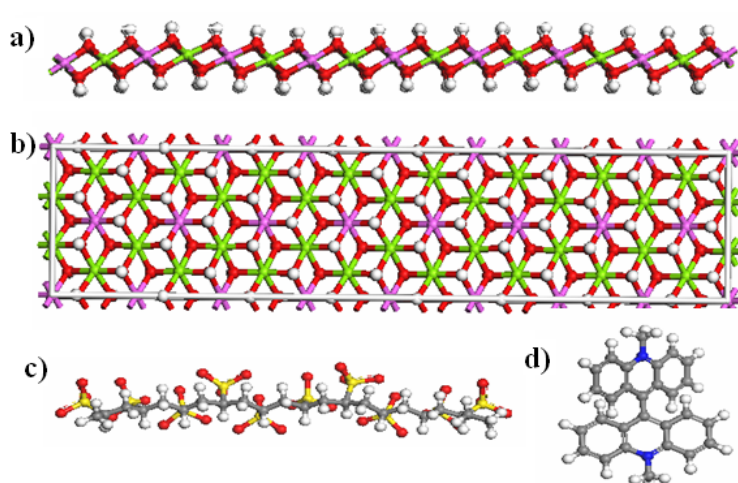


Figure S7. I-V profiles for the $(\text{BNMA}@\text{PVS/LDH})_n$ UTF.

7. Calculation details and analysis of the (BNMA@PVS/LDH)_n system.

7.1 Building of the structural model for BNMA@PVS/LDH: An ideal LDH superlattice layer with R3-m space group containing 32 Mg atoms and 16 Al atoms was built. The distance of adjacent metal atoms in the 2-dimensional layer is 3.05 Å, which is in accordance with other literatures.^[5] A supercell was constructed with lattice parameter $a = 36.60$ Å, $b = 9.15$ Å and the initial interlayer spacing $c = 13$ Å, $\alpha = \beta = 90^\circ$, $\gamma = 90^\circ$ (equivalent to $16 \times 3 \times 1$ in the a , b , c direction, Scheme S1a, S1b). The supercell was treated as P1 symmetry and three dimensional periodic boundary condition was applied to the system. Then, two anionic PVS with 10 repeated units (2PVS^{10-} , Scheme S1c), and two BNMA cations (2BNMA^{2+} , Scheme S1d) were introduced into the simulated supercell to ensure the whole system electrically neutral. It should be noted that the ratio of the PVS and BNMA is based on that of the experiment. As a result, the formula of the simulated structure can be expressed as: $\text{Mg}_{32}\text{Al}_{16}(\text{OH})_{96}(\text{C}_{21}\text{H}_{34}\text{S}_{10}\text{O}_{30})_2(\text{C}_{28}\text{H}_{22}\text{N}_2)_2$.

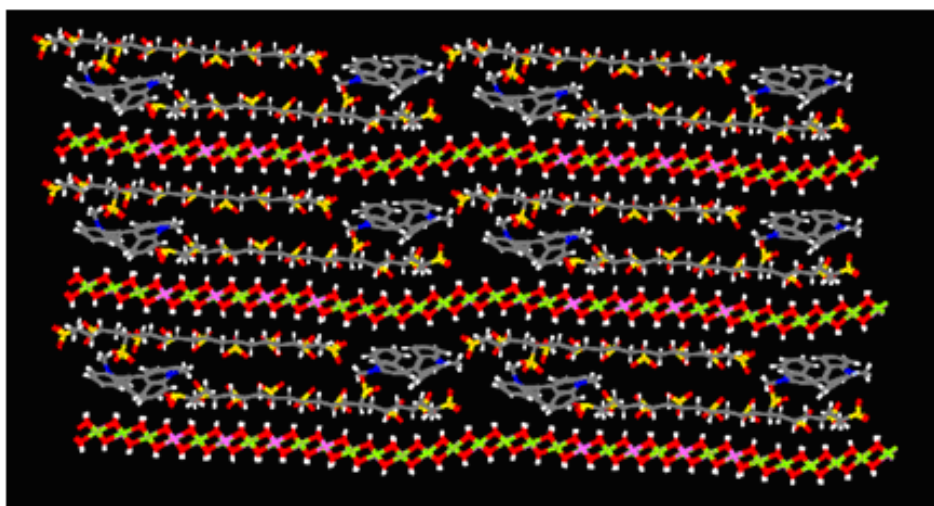


Scheme S2. (a) Side view of the $16 \times 3 \times 1$ superlattice layer, (b) top view of the superlattice layer model for Mg-Al-LDH (Color codes: white: H; red: O; pink: Al; green: Mg), (c) structural model of PVS^{10-} , and (d) structural model of BNMA^{2+} .

7.2 Computational method: A modified cff91 forcefield was employed to perform MD simulation in the whole process. Forcefield parameters for Mg, Al, O and H in the layer are fully described else.^[6] Charge Equilibration (QE) method^[7] was used to calculate atomic charges of the layer, in which the partial charges are +0.703e for Mg, +1.363e for Al, -0.537e for O and +0.243e for H. Other forcefield parameters for the anions and water molecules were referred to the cff91 forcefield.^[8] The NBO analysis^[9] was employed to calculate the partial charges of BNMA cation on B3LYP/6-31G** level using the Gaussian 03 programs.^[10] The charge of PVS polyanion was also calculated by QE method.^[7] In potential energy

calculations, the long range coulomb interactions between partial charges were computed by the Ewald summation technique^[11] and a “spline cutoff” method was used to calculate van der Waals interactions. After energy minimization was applied on the initial model, MD simulations were performed in isothermal-isobaric (NPT) ensemble with the temperature of 300 K and the pressure of 0.1 MPa (about 1 atm). The Andersen method^[12] and Berendsen method^[13] were used to control temperature and pressure, respectively. The total simulation time was 100 ps with the simulation time step of 1fs. The result shows that the system reached equilibrium with lattice parameters and total potential energy fluctuating around a constant value within the first 15-20 ps, so the dynamic trajectories were recorded every 10 fs in the remaining 80 ps in order to analyze the ensemble average values. All the simulations were performed using Discover module in Material Studio software package.^[14] The results show that the average electrostatic energy (-21055 kcal/mol) is much larger than the van der Walls interaction (887 kcal/mol), suggesting that the driving force for the UTF assembly is mainly dominated by the Coulomb interaction.

a)



b)

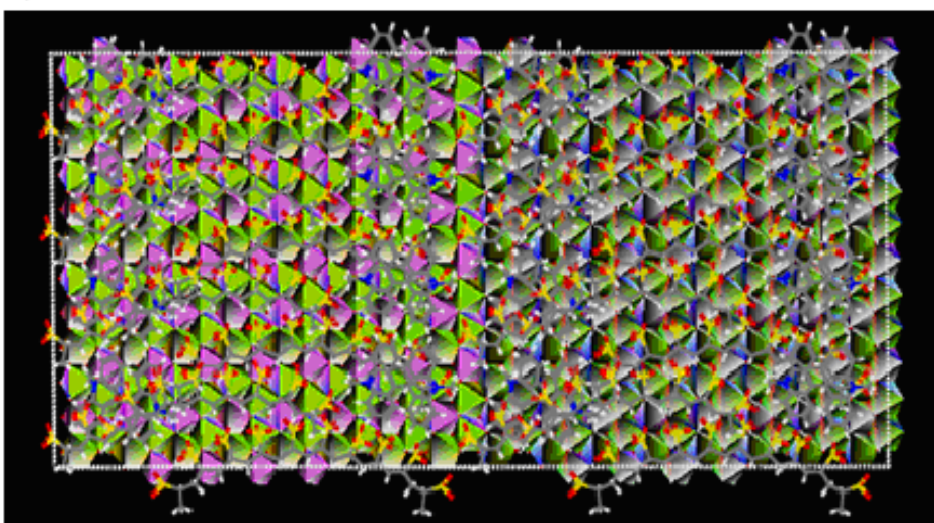


Figure S8. a) the MD snapshots of the top view, and b) side view of the BNMA@PVS/LDH system.

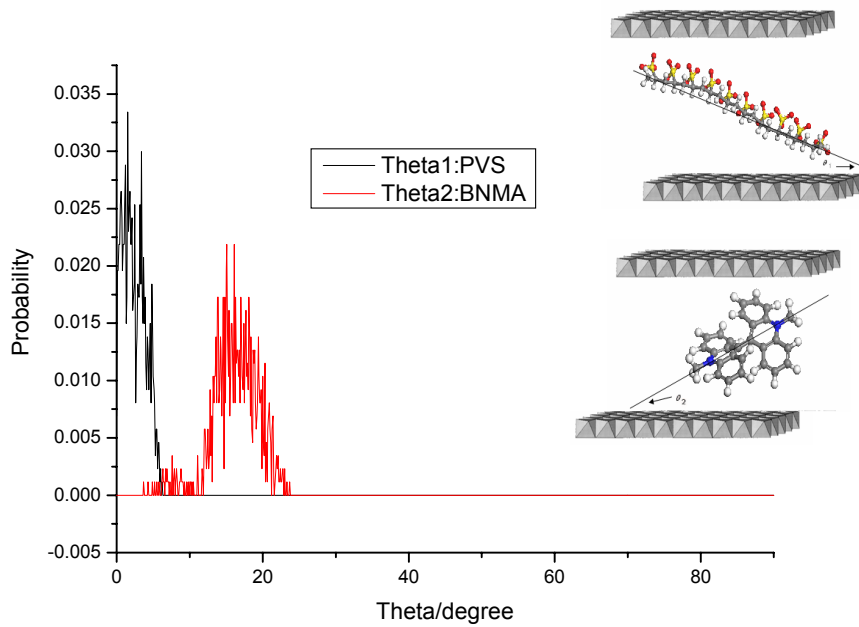
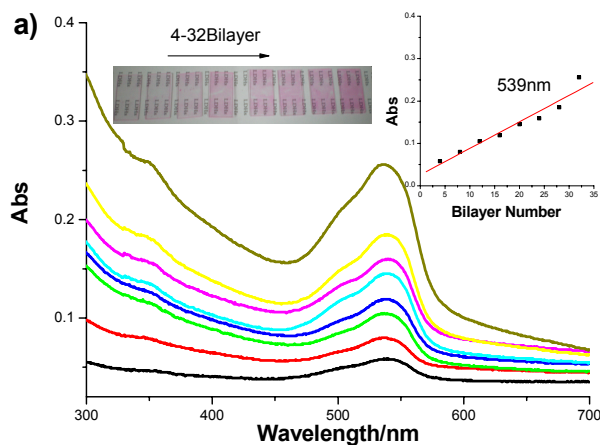


Figure S9. The angel distribution of the N–N bond in BNMA and two end-chain C–C in PVS respective to the LDH layer.

Two angles are defined to investigate the orientation of PVS and BNMA between the LDH monolayers (shown in the inset of Figure S8): angle θ_1 and θ_2 stand for the orientation angle of the lineation of two end-chain C atoms in PVS and two N atoms in BNMA respective to the layer. It was found that the most probable angle of θ_1 is 2° , and θ_2 is mainly populated at 15° , illustrating that the guest molecules adopt an ordered arrangement with a preferred orientation in the as-prepared UTF.

5. Ordered assembly of the (Rhodamine 6G@PVS/LDH)_n UTFs.



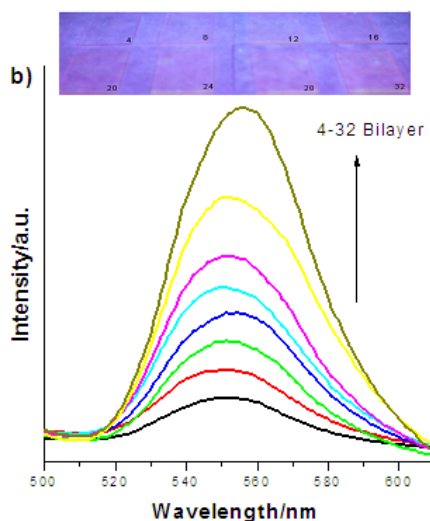


Figure S10. a) UV-Vis absorption spectra, and b) fluorescence spectra of the $(RB6G@PVS/LDH)_n$ ($n = 4\text{--}32$) UTFs. The inset in a) shows the plot of absorbance at 539 nm vs. n , the bilayer number.

The characteristic absorption band of RB6G at 539 nm linearly correlates with the bilayer number (Figure S8a). The fluorescence spectra at 555 nm also present consistent increase with the bilayer number (Figure S8b), demonstrating that the monovalent cation R6G was also assembled with LDH monolayer by a similar process. Therefore, it is expected that the method can be extended for the assembly of other functional cation and LDH system.

References:

- [1] D. P. Yan, J. Lu, M. Wei, J. B. Han, J. Ma, F. Li, D. G. Evans, X. Duan, *Angew. Chem. Int. Ed.* **2009**, *48*, 3073.
- [2] L. Mohanambe, S. Vasudevan, *J. Phys. Chem. B* **2005**, *109*, 22523.
- [3] (a) T. -Q. Nguyen, J. J. Wu, V. Doan, B. J. Schwartz, S. H. Tolbert, *Science* **2000**, *288*, 652; (b) T. -Q. Nguyen, J. J. Wu, S. H. Tolbert, B. J. Schwartz, *Adv. Mater.* **2001**, *13*, 609.
- [4] (a) B. Valeur, *Molecular Fluorescence: Principles and Applications*. Wiley-VCH, Verlag GmbH, 2001; (b) D. P. Yan, J. Lu, M. Wei, D. G. Evans, X. Duan, *J. Phys. Chem. B* **2009**, *113*, 1381.
- [5] (a) L. Mohanambe, S. Vasudevan, *J. Phys. Chem. B* **2005**, *109*, 15651; (b) L. Mohanambe, S. Vasudevan, *Langmuir* **2005**, *21*, 10735; (c) S. P. Newman, S. J. Williams, P. V. Coveney, W. Jones, *J. Phys. Chem. B* **1998**, *102*, 6710; (d) J. W. Wang, A. G. Kalinichev, R. J. Kirkpatrick, X. Q. Hou, *Chem. Mater.* **2001**, *13*, 145; (e) A. Trave, A. Selloni, A. Goursot, D. Tichit, J. Weber, *J. Phys. Chem. B* **2002**, *106*, 12291.

- [6] (a) D. P. Yan, J. Lu, M. Wei, H. Li, J. Ma, F. Li, D. G. Evans, X. Duan, *J. Phys. Chem. A* **2008**, *112*, 7671; (b) D. P. Yan, J. Lu, M. Wei, J. Ma, D. G. Evans, X. Duan, *Phys. Chem. Chem. Phys.* **2009**, *11*, 9200.
- [7] A. K. Rappé, W. A. Goddard, *J. Phys. Chem.* **1991**, *95*, 3358.
- [8] J. R. Maple, M.-J. Hwang, T. P. Stockfisch, U. Dinur, M. Waldman, C. S. Ewig, A. T. Hagler, *J. Comput. Chem.* **1994**, *15*, 162.
- [9] A. E. Reed, L. A. Curtiss, F. Weinhold, *Chem. Rev.* **1988**, *88*, 899.
- [10] M. J. Frisch, G. W. Trucks, H. B. Schlegel, G. E. Scuseria, M. A. Robb, J. R. Cheeseman, J. A. Montgomery, Jr., T. Vreven, K. N. Kudin, J. C. Burant, J. M. Millam, S. S. Iyengar, J. Tomasi, V. Barone, B. Mennucci, M. Cossi, G. Scalmani, N. Rega, G. A. Petersson, H. Nakatsuji, M. Hada, M. Ehara, K. Toyota, R. Fukuda, J. Hasegawa, M. Ishida, T. Nakajima, Y. Honda, O. Kitao, H. Nakai, M. Klene, X. Li, J. E. Knox, H. P. Hratchian, J. B. Cross, C. Adamo, J. Jaramillo, R. Gomperts, R. E. Stratmann, O. Yazyev, A. J. Austin, R. Cammi, C. Pomelli, J. W. Ochterski, P. Y. Ayala, K. Morokuma, G. A. Voth, P. Salvador, J. J. Dannenberg, V. G. Zakrzewski, S. Dapprich, A. D. Daniels, M. C. Strain, O. Farkas, D. K. Malick, A. D. Rabuck, K. Raghavachari, J. B. Foresman, J. V. Ortiz, Cui, Q. A. G. Baboul, S. Clifford, J. Cioslowski, B. B. Stefanov, G. Liu, A. Liashenko, P. Piskorz, I. Komaromi, R. L. Martin, D. J. Fox, T. Keith, M. A. Al-Laham, C. Y. Peng, A. Nanayakkara, M. Challacombe, P. M. W. Gill, B. Johnson, W. Chen, M. W. Wong, C. Gonzalez, and J. A. Pople, *Gaussian 03*: Revision B.04; Gaussian, Inc.: Pittsburgh, PA, 2003.
- [11] (a) M. P. Allen, D. J. Tildesley, *Computer Simulation of Liquids*, Clarendon, Oxford, 1987; (b) A. R. Leach, *Molecular Modeling, Principles and Applications*, Pearson Education Ltd, England, 2nd edn. 2001. (c) S. Choi, J. Coronas, E. Jordan, W. Oh, S. Nair, F. Onorato, D. F. Shantz, M. Tsapatsis, *Angew. Chem. Int. Ed.* **2008**, *47*, 552.
- [12] H. C. Andersen, *J. Chem. Phys.* **1980**, *72*, 2384.
- [13] H. J. C. Berendsen, J. P. M. Postma, A. van Gunsteren, A. DiNola, J. R. Haak, *J. Chem. Phys.* **1984**, *81*, 3684.
- [14] *Discover Module, MS Modeling*, Version 2.2; Accelrys Inc.: San, Diego, CA, 2003.